EUROPEAN ORGANIZATION FOR NUCLEAR RESEARCH

CERN-PH-EP-2005-017
26 April 2005

# Search for Superfragments and Measurement of the Production of Hyperfragments in Neutrino–Nucleus Interactions

CHORUS Collaboration

**Abstract**

A systematic search for superfragments (charmed nuclei) has been performed in 22 200 neutrino–emulsion interactions obtained with the CHORUS experiment making use of automatic off-line image analysis. The absence of candidates provides an upper limit for the superfragment production rate of $1.9 \times 10^{-4}$ (90% C.L.) relative to neutrino charged-current interactions at an average neutrino energy of 27 GeV. In the same analysis 28 hyperfragment decays were found. For the first time, a production rate of hyperfragments in neutrino–emulsion interactions was obtained. The value of the hyperfragment production rate relative to the neutrino charged-current cross-section was found to be $(2.0 \pm 0.4\,(\text{stat}) \pm 0.3\,(\text{syst})) \times 10^{-3}$.

*To be published in Nuclear Physics B*

# CHORUS Collaboration


G. Önengüt
**Çukurova University, Adana, Turkey**
R. van Dantzig, M. de Jong, R.G.C. Oldeman[1]
**NIKHEF, Amsterdam, The Netherlands**
M. Güler, U. Köse, P. Tolun
**METU, Ankara, Turkey**
M.G. Catanesi, M.T. Muciaccia
**Università di Bari and INFN, Bari, Italy**
K. Winter
**Humboldt Universität, Berlin, Germany**[2]
B. Van de Vyver[3,4], P. Vilain[5], G. Wilquet[5]
**Inter-University Institute for High Energies (ULB-VUB) Brussels, Belgium**
B. Saitta
**Università di Cagliari and INFN, Cagliari, Italy**
E. Di Capua
**Università di Ferrara and INFN, Ferrara, Italy**
S. Ogawa, H. Shibuya
**Toho University, Funabashi, Japan**
I.R. Hristova[6], A. Kayis-Topaksu[7], T. Kawamura, D. Kolev[8], H. Meinhard, J. Panman, A. Rozanov[9], R. Tsenov[8], J.W.E. Uiterwijk, P. Zucchelli[3,10]
**CERN, Geneva, Switzerland**
J. Goldberg
**Technion, Haifa, Israel**
M. Chikawa
**Kinki University, Higashiosaka, Japan**
J.S. Song, C.S. Yoon
**Gyeongsang National University, Jinju, Korea**
K. Kodama, N. Ushida
**Aichi University of Education, Kariya, Japan**
S. Aoki, T. Hara
**Kobe University, Kobe, Japan**
T. Delbar, D. Favart, G. Grégoire, S. Kalinin, I. Makhlioueva
**Université Catholique de Louvain, Louvain-la-Neuve, Belgium**
A. Artamonov, P. Gorbunov, V. Khovansky, V. Shamanov, I. Tsukerman
**Institute for Theoretical and Experimental Physics, Moscow, Russian Federation**
N. Bruski, D. Frekers
**Westfälische Wilhelms-Universität, Münster, Germany**[2]
K. Hoshino, J. Kawada, M. Komatsu, M. Miyanishi, M. Nakamura, T. Nakano, K. Narita, K. Niu, K. Niwa, N. Nonaka, O. Sato, T. Toshito
**Nagoya University, Nagoya, Japan**
S. Buontempo, A.G. Cocco, N. D'Ambrosio, G. De Lellis, G. De Rosa, F. Di Capua, G. Fiorillo, A. Marotta, M. Messina, P. Migliozzi, L. Scotto Lavina, P. Strolin, V. Tioukov
**Università Federico II and INFN, Naples, Italy**
T. Okusawa
**Osaka City University, Osaka, Japan**
U. Dore, P.F. Loverre, L. Ludovici, G. Rosa, R. Santacesaria, A. Satta, F.R. Spada
**Università La Sapienza and INFN, Rome, Italy**
E. Barbuto, C. Bozza, G. Grella, G. Romano, C. Sirignano, S. Sorrentino
**Università di Salerno and INFN, Salerno, Italy**
Y. Sato, I. Tezuka
**Utsunomiya University, Utsunomiya, Japan**

[1] Now at University of Liverpool, Liverpool, UK
[2] Supported by the German Bundesministerium für Bildung und Forschung under contract numbers 05 6BU11P and 05 7MS12P.
[3] Now at SpinX Technologies, Geneva, Switzerland.
[4] Fonds voor Wetenschappelijk Onderzoek, Belgium.
[5] Fonds National de la Recherche Scientifique, Belgium.
[6] Now at DESY, Hamburg.
[7] On leave of absence from Çukurova University, Adana, Turkey.
[8] On leave of absence and at St. Kliment Ohridski University of Sofia, Bulgaria.
[9] Now at CPPM CNRS-IN2P3, Marseille, France.
[10] On leave of absence from INFN, Ferrara, Italy.

## 1 Introduction

The possible existence of superfragments—nuclei containing a charmed baryon such as a $\Lambda_c^+$—has been described theoretically in Refs. [1]-[8]. Only one experiment has reported the observation of three superfragment candidates. These were obtained in 250 GeV/$c$ proton–emulsion interactions [9]. The existence of superfragments has still not been demonstrated experimentally in a conclusive way. On the other hand, hyperfragments—nuclei containing a strange baryon—have been vigorously studied in experiments using various reactions: (K, $\pi$), ($\pi$, K), (e, e′K), ($K^-$, $K^+$) and ($\gamma$, K) (see for example, Refs. [10]-[12] and references listed therein). The production of those states in neutrino interactions has not attracted interest in the past because of the extremely small cross-section ($\sigma/E_\nu \approx 10^{-42}\mathrm{m}^2/\mathrm{GeV/nucleon}$). However, the production fractions for charmed particles and strange particles in neutrino charged-current (CC) interactions are estimated to be approximately 6% and 20%, respectively. For the production of superfragments, the neutrino interactions have the particular advantage of a much higher production ratio for charmed particles compared to reactions of other incoming particles.

The characteristic features of hyperfragment and superfragment production in an emulsion target are the heavily ionizing track ('black track') of the fragment originating at the primary interaction vertex followed by a secondary decay vertex. From the decay vertex the daughter fragments are visible as black tracks. In non-mesic decays, uniquely black tracks are present. In mesic decays at least one of the daughter particles leaves a track compatible with a single charged particle. The characteristic decay length is expected to be of the order of several microns, well within reach of detection in an emulsion target. Therefore, in order to detect the production of hyperfragments and superfragments, the primary interaction vertex has first to be found and black tracks near to this vertex detected. The main selection criterion is then the non-zero impact parameter of at least one of these black tracks with respect to the interaction vertex, indicating the presence of a secondary vertex.

Finally, with a kinematical analysis of the decay vertex one can distinguish superfragments from hyperfragments by their much larger energy release.

The development of automatic emulsion analysis systems [13] greatly increases the ability to process large numbers of neutrino events. This progress makes it possible to detect superfragments or hyperfragments produced in neutrino–emulsion interactions. These systems, however, have not been optimized for the analysis of nuclear fragments, which are observed as black tracks in emulsion. In the neutrino–emulsion experiments performed up to now, only shower tracks ('thin tracks') produced with relativistic momenta have been studied. Hence, searching for rare events with black tracks produced in neutrino interactions still has to be conducted manually and requires much eye-scanning work even though the scanning is made easier with the help of semi-automated or fully automated emulsion analysis systems. In the CHORUS experiment, digitized video images of a large number of neutrino interaction vertices were taken during the automated emulsion analysis. Off-line image analysis reduced the emulsion-scanning load to a large extent.

In this paper, an upper limit for the production of superfragments is presented and the first measurement of the production rate for hyperfragments in neutrino–emulsion interactions is given.

## 2 Experimental procedure

The CHORUS detector [14], a hybrid setup consisting of an emulsion target and electronic detectors, was designed to search for $\nu_\mu \rightarrow \nu_\tau$ oscillation. The detector was installed in the West Area of CERN and exposed to the wide band neutrino beam of the CERN SPS (average energy 27 GeV) during the years 1994–97. The data taking was divided into two periods 1994–95 (Run I) and 1996–97 (Run II). The muon neutrino beam contains 6% $\overline{\nu}_\mu$ and 1% $\nu_e$. The integrated intensity corresponds to $5.06\times10^{19}$ protons on the production target. In this paper we present the analysis of a total of 22 200 events found by emulsion-image analysis out of 74 454 events taken in Run II. In each run, an emulsion target with a total mass of 770 kg was exposed. The emulsion was replaced after Run I. The target was segmented into four stacks, each of the stacks consisting of eight modules. A module contained 36 emulsion plates of size 36 cm $\times$72 cm which were made of a 90 $\mu$m plastic base coated on both sides with a 350 $\mu$m emulsion layer.

Events containing only one muon ($1\mu$ event) with negative charge and momentum smaller than 30 GeV/$c$ were selected for event location in the emulsion target. The selection was optimized for the

detection of decays of the $\tau$ lepton.

The emulsion-scanning procedure was performed with fully automated emulsion analysis systems. The negative muon track ('scan-back track') was followed upstream in the module from one plate to the next. If the scan-back track was not observed in two consecutive plates, the first of these plates was called the 'vertex plate' as shown in Fig. 1. The interaction vertex (primary vertex) was expected to be in this plate. For each side of the vertex plate, tomographic video images were taken by focusing at 48 different focal depths of the emulsion as illustrated in Fig. 2(a). An image of a focal plane ('frame') consisted of 512×512 pixels. A set of 48 frames ('view') covered a volume of about 150 $\mu$m × 120 $\mu$m × 350 $\mu$m. This volume was used as one unit for the image analysis. Depending on the slope of the scan-back track, a total of two, four or six views were taken in a vertex plate containing the primary vertex, as shown in Fig. 2(b). One image consisted of a set of these views. Because images were filtered by a track selector [13] (an automatic image analysis processor) in the read-out direction of the CCD camera ('scanning line') to optimize the recognition of shower tracks (minimum-ionizing particles) for the $\tau$ search, black tracks were eliminated in that direction. Thus, the image processing was insensitive to black tracks along the scanning line as shown in Fig. 3(a). The number of events corresponding to the number of images analysed are listed in Table 1.

In addition to the off-line image analysis, 1866 images of randomly selected events were checked by eye ('eye-checked images') with an image viewer displayed on a CRT-monitor screen and the primary vertex position was measured to evaluate the accuracy of the image analysis. The fraction of events of the eye-checked images containing a primary vertex is $(71.5 \pm 2.0)$%. Of the 1866 events, $(66.0 \pm 1.8)$% had their primary vertex in the emulsion material, as summarized in Table 2. Furthermore, the angles of 668 black tracks emitted from 175 interaction vertices out of the 1866 eye-checked images were manually measured in the emulsion ('emulsion-checked images') to evaluate the efficiency of finding black tracks by image analysis.

## 3 Image analysis

The image-analysis procedure is much faster than the manual eye-scanning in the emulsion and hence significantly reduces the emulsion-scanning load. The image-analysis procedure started by reconstructing clusters defined as sets of pixels adjacent to each other. The parameters of clusters were evaluated as shown in Fig. 4. The important parameters to be determined in the search for hyperfragments were centre position, best straight-line fit, 'size' (the number of pixels making up a cluster) and width. After the clustering, the image analysis proceeded in four steps.

First, a procedure to search for track segments was applied. Black tracks were searched for in the whole region of 48 frames and shower tracks (including the scan-back track) were searched for in the downstream 16 frames (110 $\mu$m), respectively, as illustrated in Fig. 5. In order to search for shower tracks, pairs of frames, seven frames apart were formed. These frames define planes at a distance of 52 $\mu$m. Eight such consecutive pairs were formed to cover the sixteen frames downstream of the primary vertex. Between each of these pairs of planes, straight lines were defined by choosing each possible combination with one cluster on either frame. The number of consecutive clusters on or close to the line was counted. The best-fit line was then obtained using these clusters and the standard deviation ($\sigma_{\mathrm{d}}$) of distance of clusters from the line was evaluated. A straight line was accepted as track segment when it contained at least six clusters each positioned on different frames and when the $\sigma_{\mathrm{d}}$ was smaller than 0.5 $\mu$m. The procedure to recognize black tracks was similar. Track segments with length greater than 40 $\mu$m (penetrating at least 6 frames) were scanned for in the whole region of 48 frames accepting clusters with size greater than 20 pixels.

As a second step, the primary vertex was reconstructed in a fiducial volume which was enclosed by planes 10 $\mu$m inside the edge on the sides, and 40 $\mu$m downstream along the beam direction from the surfaces of the view as shown in Fig. 6. In this analysis, all track segments irrespective of whether they were shower tracks or black tracks were used. Positions with distance of closest approach less than 2 $\mu$m between each combination of track segments were defined as trial vertices. Track segments passing close to the trial vertices were attached to these. The most probable primary vertex was determined by choosing the one with the maximum number of tracks and with the smallest average impact parameter of the tracks to the candidate vertex. The average impact parameter was required to be smaller than 1.5 $\mu$m.

The procedure is illustrated in Fig. 6. In cases where no such vertex was found, the point where a scan-back track was found to be within 2 $\mu$m of a cluster with size greater than 110 pixels was chosen as the primary vertex.

In total, 25 257 events with a primary vertex candidate were found as listed in Table 3. The accuracy of the vertex candidate search was evaluated by using the eye-checked images of 1866 events which contained 1097 events with a primary vertex in the fiducial volume. The automatic procedure found 567 events with a primary vertex candidates in this sample. Out of these 567 vertices 33 were fake, because no real vertex was found by the eye-scan procedure. The distribution of deviations of the position of the primary vertex between the image analysis and the manual measurements is shown for the remaining 534 events in Fig. 7. A total of 498 events out of 534 events were found within a tolerance of $|\Delta x| \leq 3$ $\mu$m, $|\Delta y| \leq 3$ $\mu$m and $|\Delta z| \leq 15$ $\mu$m. The probability of finding a vertex by chance within this region is $10^{-4}$ per event. The positions obtained by the image analysis were in good agreement with the manual measurements. The finding efficiency of the primary vertex in the fiducial volume within $|\Delta x| \leq 3$ $\mu$m, $|\Delta y| \leq 3$ $\mu$m and $|\Delta z| \leq 15$ $\mu$m is estimated to be $(45.4 \pm 2.1)$%. Using these numbers, the number of actual primary vertices found in the fiducial volume by image analysis is evaluated to be $(22.2 \pm 1.0) \times 10^3$.

A search for hyperfragment decays was performed as a third step in the procedure. The detection of hyperfragments required that at least one black prong coming from the primary vertex ('candidate black track') be picked up. These were searched for and divided into two categories: tracks reconstructed in three dimensions (3D track), and tracks observed as an aligned cluster of pixels in one or only a few frames (2D track). The latter tracks could not be reconstructed three-dimensionally. This situation occurs if the angle of the black track with respect to the beam direction is large.

For 3D tracks it was required that the distance ($D_z$) to the vertex in the beam direction at the position of closest approach to the vertex be greater than 4 $\mu$m or that the impact parameter ($D$) to the vertex projected on a plane perpendicular to the beam be greater than 2 $\mu$m and less than 20 $\mu$m as shown in Fig. 8(a). These requirements were imposed only on tracks with an angle less than 1.0 rad. The clusters of 2D tracks were inspected frame-by-frame as shown in Fig. 8(b). Clusters with size greater than 140 pixels (10 $\mu$m$^2$) were examined in the frames within a distance of 30 $\mu$m from the primary vertex along the beam direction. The following selection criteria were applied:

- The width of the cluster was required to be greater than 2.5 $\mu$m.
- The impact parameter ($D_{\min}$) with respect to the vertex projected onto the frame was within a 1.5 $\mu$m to 30 $\mu$m interval. The upper limit was applied to reduce random background.

Because nuclear fragments were close to each other and their tracks not separated in the vicinity of the primary vertex, a region with a radius less than 1.5 $\mu$m from the primary vertex was excluded from the analysis.

Out of 25 257 events 14 733 events were removed from further analysis because no candidate black tracks were found. For the remaining 10 524 events most of the candidate black tracks were removed after inspection. They were recognized as background tracks with characteristics such as low-momentum curving tracks, scattering tracks, nuclear fragments coming from the primary vertex with a $\delta$-ray, $\alpha$-particle or heavier fragment, or combinatorial background of black tracks not related to the event. Since it was difficult to recognize these as background with the off-line image analysis, the last step of the analysis, the 'image-check', was performed for these events. The images were checked by eye with an image viewer where the clusters of interest were colour-coded on a graphics monitor. The image check was done for 10 524 events in which the candidate black tracks were found. After having been recognized as belonging to the above-mentioned types of background 10 262 events were removed from further analysis. The results of the image check are summarized in Table 3.

## 4 Emulsion check procedure and selection of candidates

The 262 events selected by the image check were carefully inspected in the emulsion (*i.e.* directly under the microscope). One-prong decay topologies were excluded from the analysis because of the difficulty of identification as hyperfragments. The selected events were inspected for the following visual features:

- The number of prongs from the secondary vertex was greater than or equal to two including at least one black track.
- The track connecting the primary vertex and the secondary vertex was black.
- The connecting track was not distinguished as black or thin in cases where the secondary vertex was very close to the primary vertex with distance less than 5 $\mu$m, because the vicinity of the vertices was obscured by tracks emitted from these.

A total of 33 candidates were found with their secondary vertex within a distance of 50 $\mu$m from the primary vertex. For the candidate events, all tracks from the secondary vertices were followed to the end of their range or until they left the module (emulsion stack), and the emission angle and the range of the tracks in the module were measured.

Five out of 33 candidates were removed since they can be attributed to background processes as described below. Two events with a two-prong topology were consistent with nuclear elastic scattering. One three-prong event with a length of 3.6 $\mu$m was identified as $\Lambda_c^+ \to \Sigma^+\pi^+\pi^-(\pi^0)$ with a subsequent $\Sigma^+ \to n\pi^+$ decay. In this event, the characteristic $\pi^+ \to \mu^+ \to e^+$ decay chains of the two $\pi^+$'s (one from $\Lambda_c^+$ decay and the other from $\Sigma^+$ decay) were observed and the measured topology was kinematically consistent with $\Lambda_c^+$ decay. Two events were identified, respectively, as nuclear capture of a slow $\pi^-$ meson ($\sigma$-star) and a $K^-$ capture.

For 26 of the remaining 28 hyperfragment candidates, all decay prongs stop in the emulsion and can be identified as protons or heavier nuclear fragments. Figure 9 shows an example of one of the candidates. A kinematical analysis was performed to check whether the events were consistent with the hypothesis of a non-mesic decay at rest of a light hyperfragment (up to $Z = 8$). All the combinations of possible mass assignments were considered for the decay prongs. For each of these combinations, the visible momentum was evaluated using the direction and the range of the decay prongs, and, if not compatible with zero within the errors, a minimum number of neutrons was assumed to carry the missing momentum. In this analysis, no events interpreted as a decay into only charged particles were found. Using the known values of the binding energy of the light hyperfragment species, the energy release was then evaluated and compared to the visible energy (corrected for the neutron energy where appropriate). In all cases except one, at least one combination was found to be compatible with the decay mode hypothesis if only one neutron was assumed. The remaining one was consistent with the decay hypothesis assuming two neutrons. No superfragment candidate with an energy release exceeding that for hyperfragments (176 MeV) has been found.

For two events in which one of the decay prongs escaped the emulsion module, the nature of the daughter particles could not be determined in the same way. However, since the kinetic energy of a $\pi^-$ produced in a mesic decay is expected to be approximately 30 MeV [15] reflecting that of $\Lambda^0$ decay, it is expected to be observed as a track with an ionization around 1.7 times that of a minimum-ionizing particle ('mip') in the emulsion. The two out-going tracks were observed to be grey tracks with ionization significantly exceeding 1.7 mip, thereby ruling out the assignment of a $\pi^-$ from a mesic decay. The general features of the hyperfragment events are summarized in Table 4 and the range distribution is shown in Fig. 10(a).

## 5 Background estimation

Nuclear fragments from the primary vertex cannot cause the desintegration of another nucleus at the end of their range because they have nearly zero energy. Decays of heavy fragments $^8\mathrm{Li} \to {}^8\mathrm{Be}\,\beta^-\nu$, $^8\mathrm{Be}^* \to 2\alpha$ (so-called 'hammer tracks') can easily be distinguished from other fragments by their characteristic feature. Twelve hammer tracks were found. Possible background sources to the superfragment and hyperfragment search are $\sigma$-stars, secondary interactions by shower tracks producing black prongs and a slow $\Lambda_c^+$ decay with grey or black decay prongs.

These background events can generally be distinguished from hyperfragments by their large amount of multiple scattering observed near the secondary vertex or a singly charged connecting track if their range is greater than 10 $\mu$m. In our analysis, one $\sigma$-star and two secondary interactions were found with range $R$ within $10\ \mu\mathrm{m} \leq R \leq 50\ \mu\mathrm{m}$. For short ranges ($R \leq 10\ \mu$m) it is difficult to exclude these backgrounds. However, it has been reported in an early emulsion experiment using a $\pi^-$ beam that no events interpreted as hyperfragments were observed below the threshold for $\Lambda^0$ production [16]. Hence

we expect that the background from candidates with short ranges is small.

The remaining background events are mostly slow $\Lambda_c^+$ decays. All hyperfragment candidates except the one mentioned in the previous section were identified as not being $\Lambda_c^+$ decay because each had more than two heavy prongs which stopped in the emulsion and were distinguished from $\pi$ and K. The range distribution of secondary vertices which were identified as not being hyperfragments is shown in Fig. 10(b).

The expected number of $\sigma$-stars and secondary interactions with range less than 10 $\mu$m was estimated to be 0.25$\pm$0.25 and 0.30$\pm$0.07, respectively, assuming that the probability of these background events occurring is proportional to the track length. The total background expected in the hyperfragment candidate event sample is estimated to be 0.6$\pm$0.3.

## 6 Detection efficiency for hyperfragments

A comparison was made of the emulsion-checked images and the image analysis to evaluate the efficiency of finding black tracks. The efficiency as shown in Fig. 11 depends on the azimuthal angle because an image filtering was performed in the direction of the scanning line of the CCD camera to eliminate non-minimum-ionizing tracks and to optimize the finding of shower (thin) tracks. The efficiency for the detection of hyperfragments has been evaluated with a Monte Carlo simulation. The following effects were considered:

- The distribution of the primary vertex position in the image.
- The deviation of the primary vertex position determined by the image analysis from the actual position as shown in Fig. 7.
- The assumption that the hyperfragment was emitted isotropically from the primary vertex.
- The assumption that each decay prong was emitted isotropically at the end of the range of the hyperfragment without correlation with the other prongs.
- The efficiency of finding black tracks as shown in Fig. 11.

In Fig. 12(a) the result of the efficiency evaluation is shown as a function of range. The calculated efficiency was checked by analysing 'stars' associated with five or four prongs with length around 30 $\mu$m which are expected to be due to $\alpha$-decays of radioactive contaminations like $^{228}$Th. These are distributed uniformly in the emulsion. The density was measured to be 4.32$\pm$0.51stars/mm$^3$. These stars were also found as hyperfragment candidates in the scanning stage of the image analysis. Figure 12(b) shows the distribution of distance from the primary vertex and the stars found by the image analysis. The calculated efficiency reproduces the measured distribution well.

## 7 Results

A total of 28 non-mesic hyperfragments were found. The actual number of primary vertices found by the image analysis was estimated to be (22.2$\pm$1.0)$\times 10^3$. The production fraction of hyperfragments in neutrino–emulsion interactions is given by:

$$\frac{\sigma(\nu_\mu \mathrm{A} \to \mathrm{HF}\mu^- X)}{\sigma(\nu_\mu \mathrm{A} \to \mu^- X)} = \frac{\sum_i \sum_j \{N_{ij}^{\mathrm{exp}}(\mathrm{HF}) \cdot \varepsilon_{ij}^{-1} \cdot \Delta r\}}{N^{\mathrm{exp}}(\mathrm{CC})} \cdot \frac{\varepsilon(\mathrm{CC})}{\varepsilon(\mathrm{HF})} ,$$

where:

- $i$ is the number of prongs from hyperfragment decay,
- $j$ is a range interval $r_j$ and $r_j + \Delta r$,
- $N_{ij}^{\mathrm{exp}}(\mathrm{HF})$ is the number of observed hyperfragments from which the average background is subtracted,
- $\varepsilon_{ij}$ is the average finding efficiency of hyperfragments with prong number $i$ and range interval $j$; the weighted average efficiency for this sample is $0.55 \pm 0.04$,
- $N^{\mathrm{exp}}(\mathrm{CC})$ is the estimated number of primary vertices found by the image analysis in the fiducial volume,
- $\varepsilon(\mathrm{CC})/\varepsilon(\mathrm{HF})$ is the ratio of finding efficiencies for CC events to that for hyperfragment (HF) events and is estimated to be $0.87 \pm 0.10$. The finding efficiency of the primary vertex depends weakly

on the number of shower tracks as well as on the number of nuclear fragments ($N_{\rm b}$) at the primary vertex. It is observed that the average $N_{\rm b}$ is larger for HF events than for CC events. The fact that the ratio $\varepsilon$(CC)/$\varepsilon$(HF) is different from unity is mainly due to the different distribution of $N_{\rm b}$ in HF events and CC events. The error is evaluated from the standard deviation of the $N_{\rm b}$ distribution for HF events listed in Table 4.

The ratio of non-mesic hyperfragment production to the CC interaction cross-section is determined to be:

$$\frac{\sigma(\nu_\mu \mathrm{A} \rightarrow \mathrm{HF(non\text{-}mesic)}\mu^- X)}{\sigma(\nu_\mu \mathrm{A} \rightarrow \mu^- X)} = (2.0 \pm 0.4\ (\mathrm{stat}) \pm 0.3\ (\mathrm{syst})) \times 10^{-3}\ .$$

This ratio is of the same order as the one for $s\bar{s}$ associated production in other emulsion experiments [9], [17]. The systematic error is due to the uncertainty in the efficiency of finding a hyperfragment mainly in the region within a few microns from the primary vertex where the tracks are not clearly visible and also due to the uncertainty in the distribution of $N_{\rm b}$ for HF events.

Assuming that the distribution of the range of superfragments is the same as that of hyperfragments and taking into account the average detection efficiency, the following upper limit for the ratio of superfragment production with respect to the CC interaction cross-section is obtained:

$$\frac{\sigma(\nu_\mu \mathrm{A} \rightarrow \mathrm{SF}\mu^- X)}{\sigma(\nu_\mu \mathrm{A} \rightarrow \mu^- X)} < 1.9 \times 10^{-4} \quad (90\%\ \mathrm{C.L.})\ .$$

In this limit the 15% systematic error has been taken into account following the procedure of Ref. [18].

Since the $\Lambda_{\rm c}^+$ production ratio to CC interaction is obtained to be $(1.54 \pm 0.35\ (\mathrm{stat}) \pm 0.18\ (\mathrm{syst})) \times 10^{-2}$ [19], an upper limit for the ratio of superfragment production with respect to $\Lambda_{\rm c}^+$ production in CC neutrino interactions is determined to be:

$$\frac{\sigma(\nu_\mu \mathrm{A} \rightarrow \mathrm{SF}\mu^- X)}{\sigma(\nu_\mu \mathrm{A} \rightarrow \Lambda_c^+ \mu^- X)} < 1.3 \times 10^{-2} \quad (90\%\ \mathrm{C.L.})\ ,$$

taking into account the systematic error of 30% including the additional uncertainty of the $\Lambda_{\rm c}^+$ production cross-section measurement following Ref. [18].

In our image analysis, the region close to the primary vertex with a radius less than a few microns is insensitive to the superfragment search. If we take into account the fact that the lifetime of a charmed particle is shorter than that of a strange particle and thus the range of superfragments is expected to be correspondingly shorter, the upper limits will be less stringent.

## 8 Conclusions

A systematic seach for superfragments was performed in 22 200 neutrino–emulsion interactions. Limits of the ratio of superfragment production to the CC interaction cross-section and to $\Lambda_{\rm c}^+$ production in CC neutrino interactions were obtained. In the same search, 28 hyperfragments were found. This is the first determination of the production ratio of non-mesic hyperfragments in neutrino–emulsion interactions.

It should be emphasized that, though the experiment was optimized for shower tracks and hence inefficient for black tracks, a systematic study of nuclear fragments produced in the neutrino–nucleus interactions has been achieved for the first time with automatic image analysis and a statistically meaningful number of hyperfragments were detected. This means that neutrino–emulsion interactions are expected to become very important reactions for the study of superfragments. If the automated emulsion analysis systems are optimized for black tracks, the statistics of the measurement can be significantly increased.

**Acknowledgements**

We gratefully acknowledge the help and support of the neutrino beam staff and of the numerous technical collaborators who contributed to the detector construction, operation, emulsion pouring, development, and scanning. The experiment was made possible by grants from the Institut Interuniversitaire des Sciences Nucléaires and the Interuniversitair Instituut voor Kernwetenschappen (Belgium), the Israel

Science Foundation (grant 328/94) and the Technion Vice President Fund for the Promotion of Research (Israel), CERN (Geneva, Switzerland), the German Bundesministerium für Bildung und Forschung (Germany), the Institute of Theoretical and Experimental Physics (Moscow, Russia), the Istituto Nazionale di Fisica Nucleare (Italy), the Promotion and Mutual Aid Corporation for Private Schools of Japan and Japan Society for the Promotion of Science (Japan), the Korea Research Foundation Grant (KRF-2003-005-C00014) (Republic of Korea), the Foundation for Fundamental Research on Matter FOM and the National Scientific Research Organization NWO (The Netherlands), and the Scientific and Technical Research Council of Turkey (Turkey). We gratefully acknowledge their support.

**References**


[1] C. B. Dover, S. H. Kahana and T. L. Trueman, *Phys. Rev*. **D16** (1977) 799.
[2] C. B. Dover and S. H. Kahana, *Phys. Rev. Lett.* **39** (1977) 1506.
[3] S. Iwao, *Lett. Nuovo Cim*. **19** (1977) 647.
[4] R. Gatto and F. Paccanoni, *Nuovo Cim*. **46A** (1978) 313.
[5] N. N. Kolensnikov *et al*., *Sov. J. Nucl. Phys*. **34** (1981) 533.
[6] G. Bhamathi, *Phys. Rev*. **C24** (1981) 1816.
[7] H. Bando and M. Bando, *Phys. Lett*. **109B** (1982) 164.
[8] S. A.Bunyatov et al., *Sov. J. Part. Nucl.* **23** (1992) 253.
[9] V. V. Lyukov, *Nuovo Cim*. **102A** (1989) 583.
[10] H. Bando, *Prog. Theor. Phys. Suppl*. **81** (1985) 1.
[11] B. F. Gibson, *Nuovo Cim.* **102A** (1989) 367.
[12] B. F. Gibson and E. V. Hungerford III, *Phys. Rep*. **257** (1995) 349.
[13] S. Aoki *et al*., *Nucl. Instrum. and Meth*. **B51** (1990) 446.
[14] E. Eskut *et al*., *Nucl. Instrum. and Meth*. **A401** (1997) 7.
[15] J. Sacton, *Nuovo Cim*. **15** (1960) 110.
[16] W. F. Fry and D. C. Wold, *Phys. Rev*. **104** (1956) 1473.
[17] J. Schneps *et al*., *Phys. Rev*. **106** (1957) 1062.
[18] R. D. Cousins and V. L. Highland, *Nucl. Instrum. and Meth*. **A320** (1992) 331.
[19] A. Kayis-Topaksu *et al*., *Phys. Lett*. **B555** (2003) 156.

Table 1: Number of events corresponding to the number of images analysed

| | **Images** | **Events** | **1$\mu$ events** |
|---|---|---|---|
| Run96 | 49 966 | 39 162 | 39 162 |
| Run97 | 48 767 | 40 068 | 35 292 |
| Total | 98 733 | 79 230 | 74 454 |

Table 2: Details of the analysis of images by the eye-check

| | **Events** |
|---|---|
| Eye-checked | 1866 |
| Containing primary vertex | 1335 |
| (in the emulsion) | 1241 |
| (in the base) | 94 |
| Primary vertex in the fiducial volume | 1097 |

Table 3: Results of the image analysis

| | **Events** |
|---|---|
| Events analysed (1$\mu$ events) | 74 454 |
| Found primary vertex candidates | 25 257 |
| Found candidate black track | 10 524 |
| Surviving after emulsion check | 262 |

Table 4: General features of hyperfragment candidates, where $N_{\mathrm{S}}$, $N_{\mathrm{g}}$, and $N_{\mathrm{b}}$ are the number of shower, grey, and black tracks at the primary vertex, respectively, $R_{\mathrm{HF}}$ the range of the hyperfragment, $N_{\mathrm{p}}$ the number of prongs at the secondary vertex and $R_{\mathrm{prong}}$ the range of the daughter prongs.

| | **Primary vertex** | | | **Secondary vertex** | | |
|---|---|---|---|---|---|---|
| Event | $N_{\mathrm{s}}$ | $N_{\mathrm{g}}$ | $N_{\mathrm{b}}$ | $R_{\mathrm{HF}}$ | $N_{\mathrm{p}}$ | $R_{\mathrm{prong}}$ ($\mu$m) |
| 51631132 | 5 | 1 | 4 | 2.5 | 3 | 157, 1097, 327 |
| 53673748 | 2 | | 7 | 2.3 | 4 | 153, 139, 163, 1357 |
| 53834444 | 1 | 1 | 10 | 8.4 | 4 | 119, 300, 3042, 2506 |
| 56431728 | 4 | 3 | 14 | 3.1 | 2 | 3.7, 5817 |
| 60843716 | 3 | 1 | 10 | 4.9 | 2 | 829, 967 |
| 61413914 | 5 | 2 | 11 | 3.9 | 3 | 133, 201, 1084 |
| 61490764 | 7 | | 6 | 3.3 | 3 | 62, 62, 86 |
| 62471849 | 9 | 3 | 17 | 7.4 | 5 | 7.0, 27, 179,5500, 465 |
| 62710567 | 6 | 2 | 10 | 3.7 | 3 | 210, 92, $> 1.14 \times 10^4$ (out of module) |
| 63830938 | 5 | 2 | 11 | 2.8 | 3 | 175, 461, 2021, blob |
| 64261788 | 7 | | 10 | 4.4 | 3 | 37.4, 235, 16438 |
| 64381436 | 5 | | 11 | 44 | 4 | 2.3, 43, 138, 253 |
| 65454258 | 4 | | 10 | 5.0 | 2 | 156, 181, blob |
| 65941591 | 7 | 3 | 12 | 4.3 | 2 | 956, 655 |
| 66821530 | 3 | | 12 | 8.7 | 2 | 7524, 1266 |
| 70231098 | 5 | | 10 | 1.6 | 3 | 221, 393, 358 |
| 71371272 | 5 | 2 | 9 | 3.3 | 2 | 1833, >4817 (out of module) |
| 73660464 | 9 | 2 | 14 | 6.1 | 3 | 53.8, 241.9, 98.0 |
| 75779824 | 1 | | 12 | 45 | 2 | 287, 318 |
| 76090364 | 9 | | 8 | 8.4 | 3 | 112, 98, 236 |
| 76273799 | 5 | | 2 | 39 | 3 | 2934, 64, 42 |
| 78480676 | 3 | | 16 | 33 | 4 | 9.6, 140, 163, 788 |
| 79839619 | 7 | 1 | 12 | 5.6 | 3 | 379, 5043, 318 |
| 80331217 | 7 | 1 | 7 | 4.2 | 3 | 9422, 242, 49 |
| 81126567 | 3 | | 4 | 5.6 | 3 | 15.0, 7.0, 492 |
| 81288152 | 2 | 1 | 6 | 11.0 | 4 | 519, 749, 582, 450 |
| 81430390 | 7 | | 3 | 33 | 4 | 39, 17, 269, 404 |
| 81811986 | 2 | 4 | 6 | 35 | 3 | 23, 23, 126 |

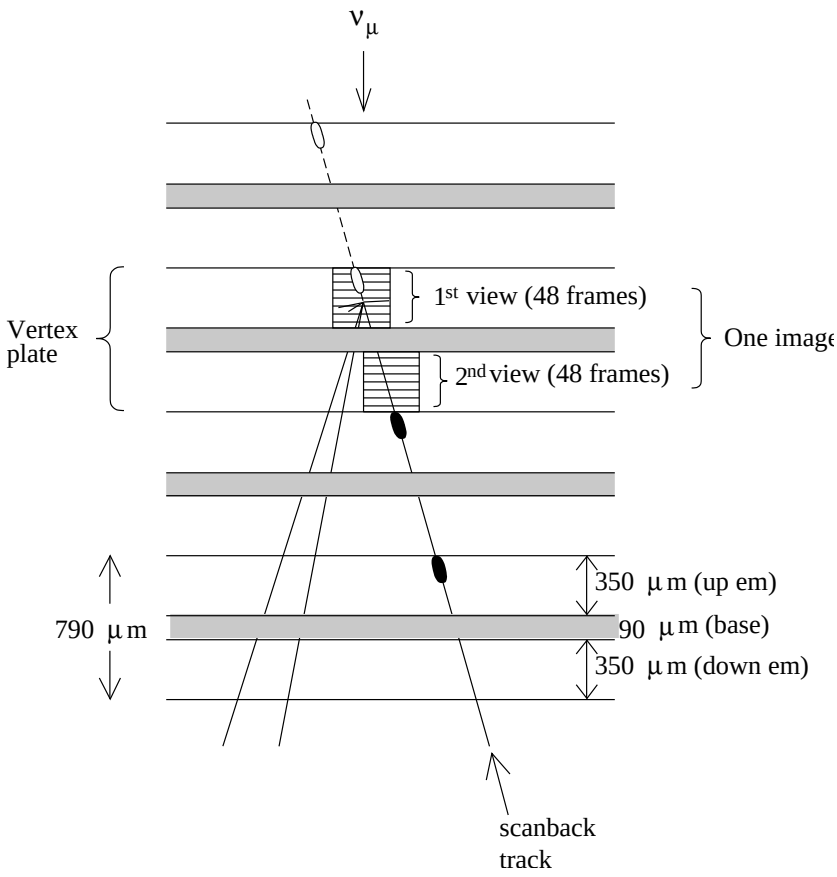


Figure 1: Vertex location. The white and black ellipses represent not found and found track segments, respectively.

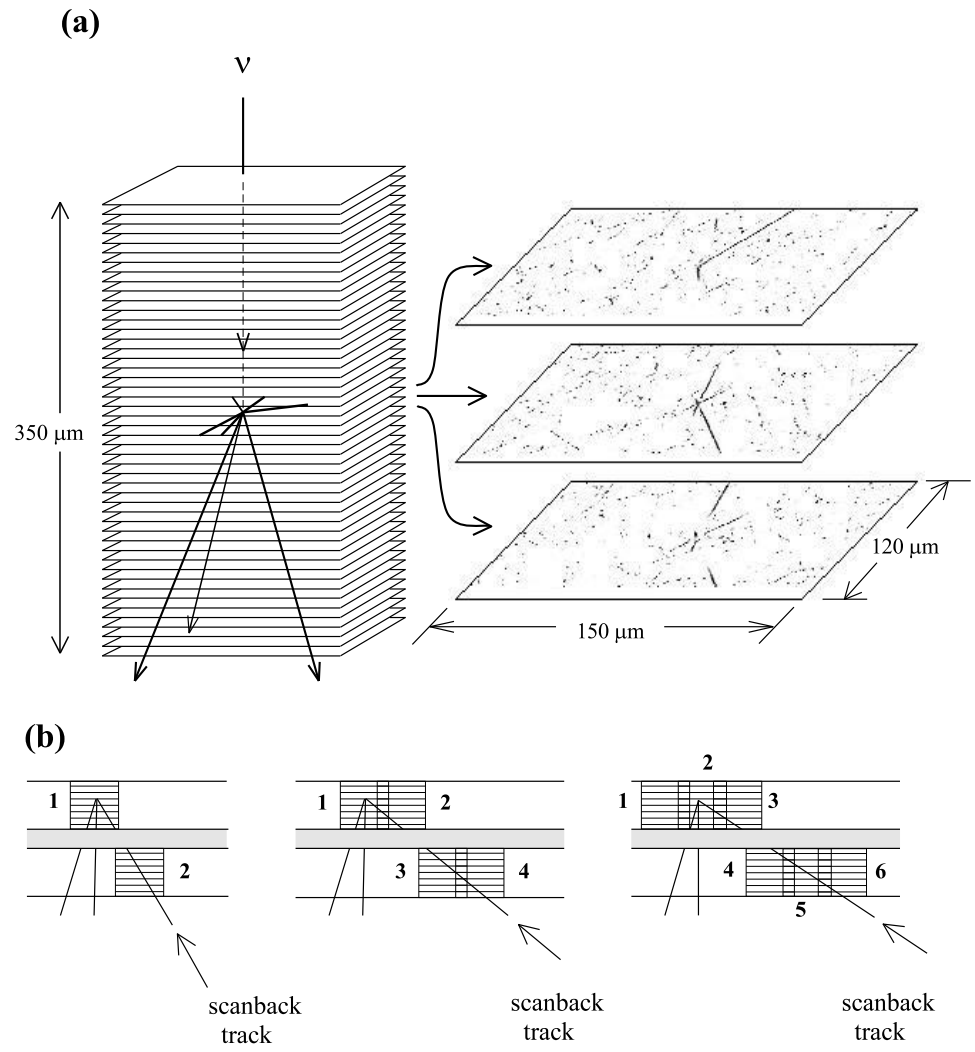


Figure 2: Construction of an image. (a) Configuration of a view. One view consists of 48 frames. (b) Configuration of an image. The integer number shows the number of the view. One image consisted of 2, 4 or 6 views corresponding to the slope of the scan-back track.

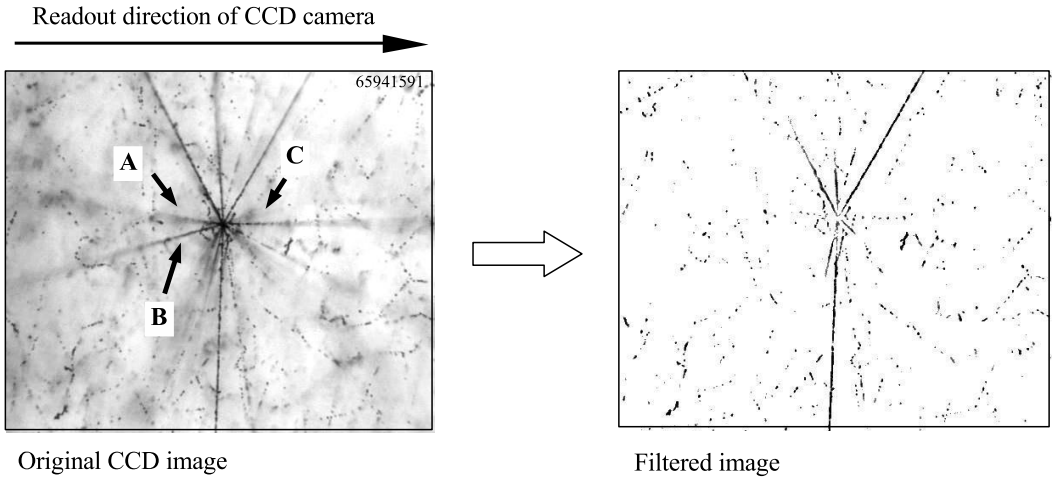


Figure 3: An example of an image. The size is $150\ \mu\mathrm{m} \times 120\ \mu\mathrm{m}$. Left-hand figure: Original CCD image. Right-hand figure: Image which was saved to be analysed after digitization and filtering. Black tracks A, B and C in the original CCD image along the direction of scanning line were eliminated in the image.

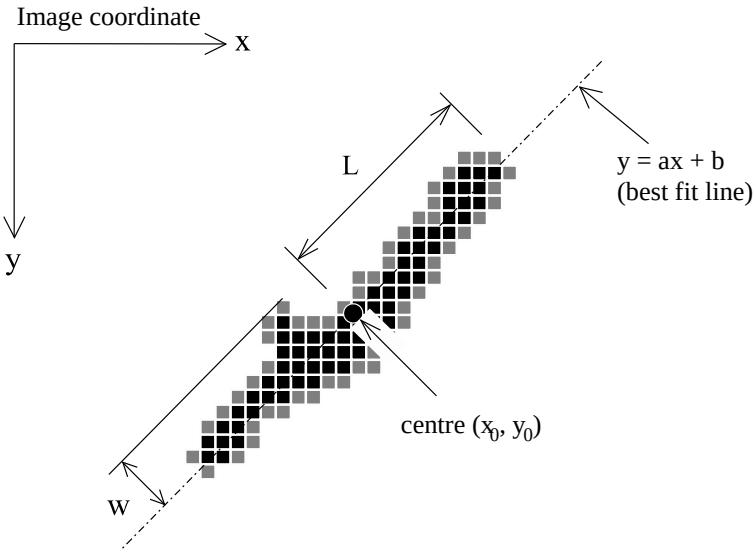


Figure 4: Parameters of a cluster.

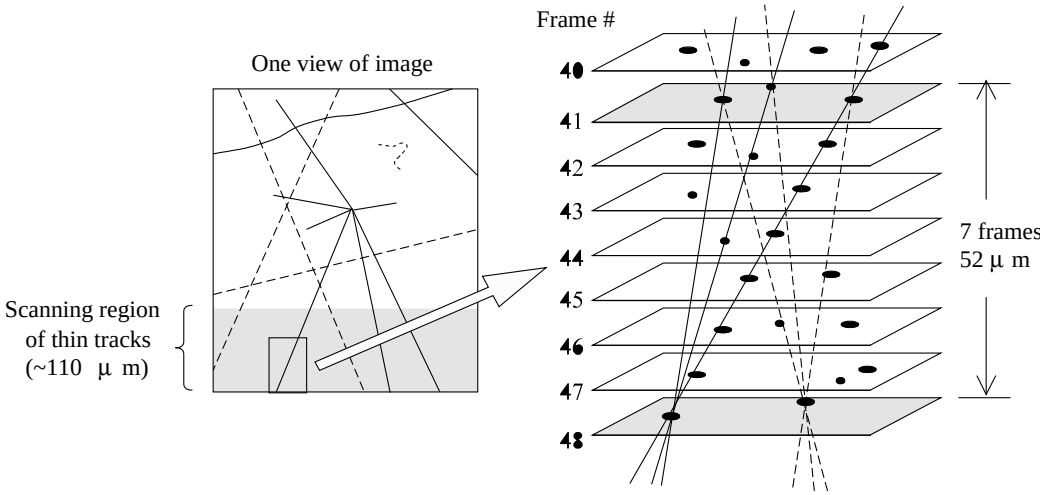


Figure 5: Schematic view of track-segment search. In this figure, six lines are formed by combining one of the two clusters in frame number 48 and one of the three clusters in frame number 41. It is recognized that only one of the six lines is a real track by counting the number of clusters on the line (indicated as thick line). The search is repeated in the same manner for the next two frames (number 47 and number 40, and so on).

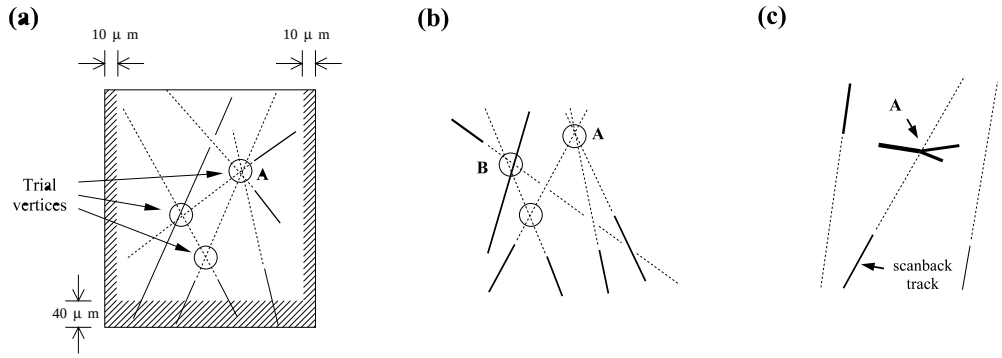


Figure 6: Schematic view of the primary vertex search. The white area indicates the fiducial volume and the broken lines denote the extrapolation of track segments. In case (a), left, the primary vertex is uniquely determined. The number of tracks forming the vertex denoted by A is maximum. (b): In case more vertices have the same number of tracks as the vertex as indicated by A, the one with the minimum impact parameter is defined as primary vertex. (c): In case no trial vertex is found, the point labelled A where the scan-back track is close to a cluster of large size is defined as primary vertex.

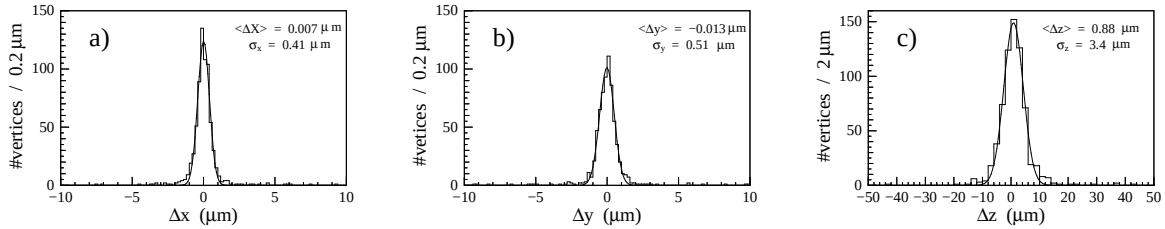


Figure 7: Distribution of the position difference of the primary vertex between image analysis and manual measurement. $x(y)$ is parallel (perpendicular) to the scanning line of the CCD camera. $z$ is the beam direction.

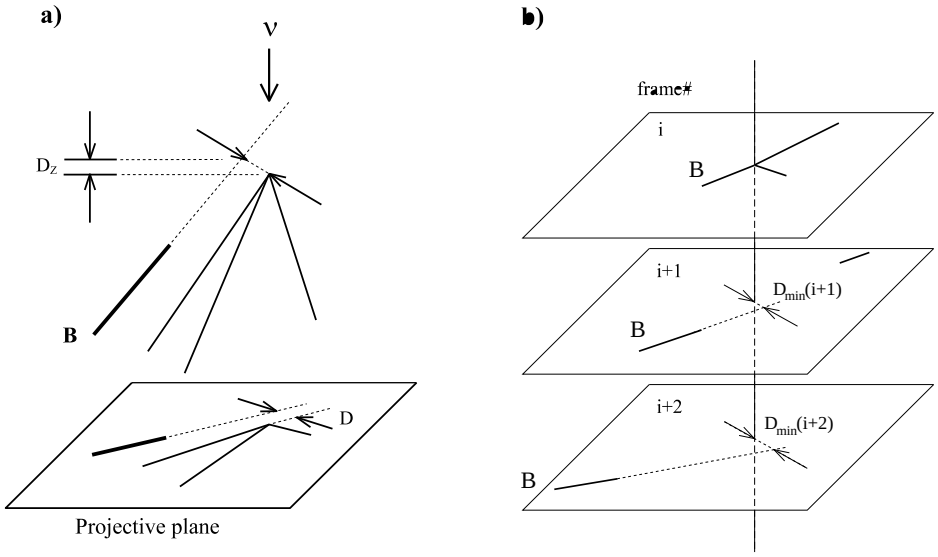


Figure 8: Illustration of the hyperfragment search. For each black track found in the image it was determined whether its extrapolation missed the primary vertex or not. The track with a significant impact parameter is denoted by B. In (a) the procedure is shown for a 3D track, in (b) for a 2D track.

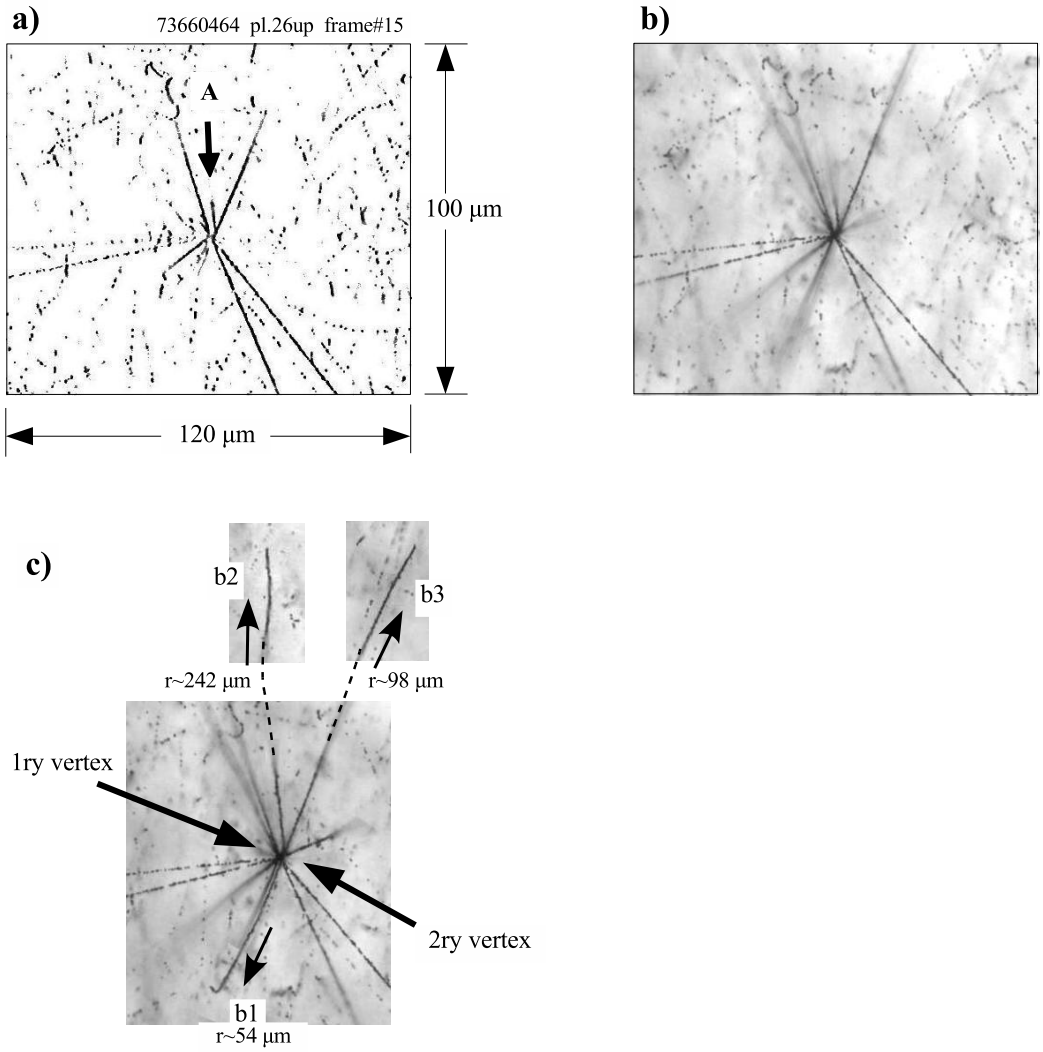


Figure 9: An example of a hyperfragment candidate. (a) A frame of the image containing the primary vertex. The candidate black track is denoted by A. (b) Unprocessed CCD image. (c) General feature of the event (composite of several focal planes). The range of the connecting track is 6.1 $\mu$m.

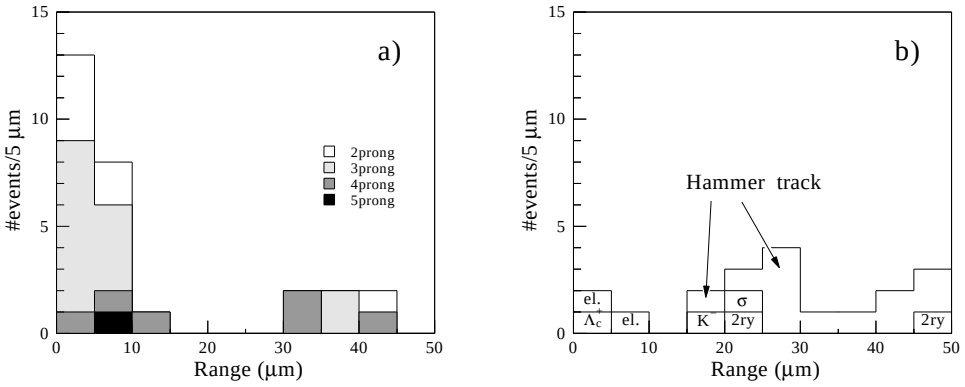


Figure 10: Range distribution. (a) Hyperfragment candidates. The grey scale of the boxes shows the number of prongs. (b) The range for tracks with secondary vertices identified as not being a hyperfragment decay.

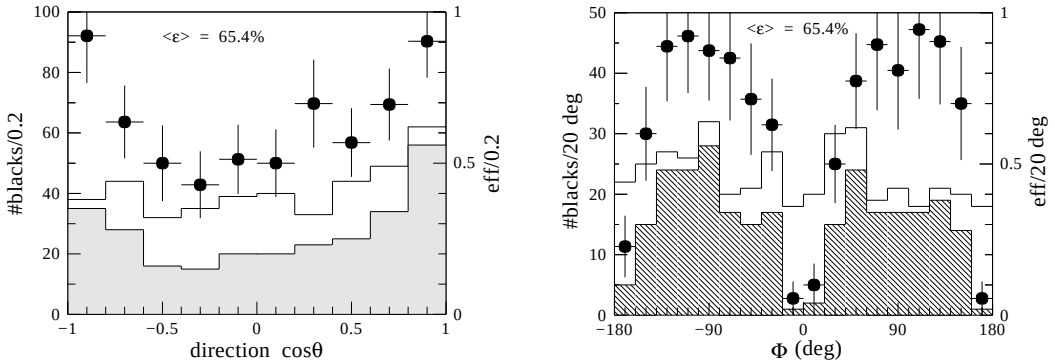


Figure 11: Black track finding efficiency. The plain histogram and the hatched histogram denote the angular distribution of all black tracks measured in the emulsion and of black tracks found by the image-analysis procedure, respectively. Black circles indicate the efficiency. Left-hand figure: The efficiency as a function of the direction $\cos\theta$ ($\theta$ is the angle with respect to the $\nu$ beam). Right-hand figure: The efficiency as a function of the azimuthal angle $\phi$. ($\phi$ is the angle with respect to the scanning line of the CCD camera.) The efficiency is low around 0 degrees and around $\pm$180 degrees due to filtering as shown in Fig. 3.

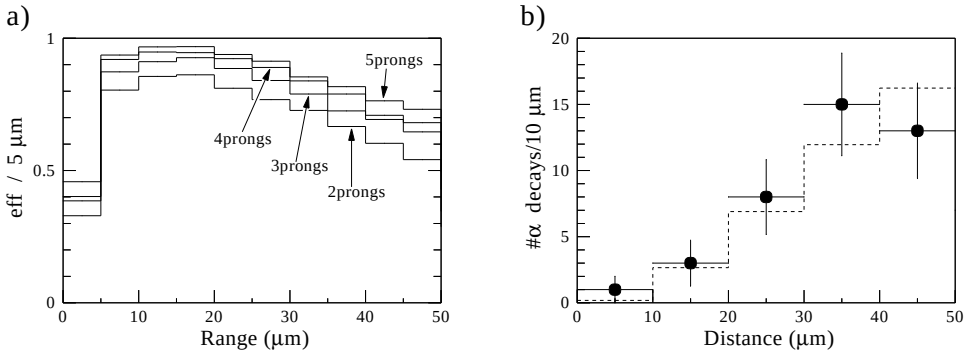


Figure 12: (a) Detection efficiency for hyperfragments. The different lines show the distribution for the different number of prongs at at the decay vertex. (b) Check of the efficiency evaluation. The black circles indicate the distribution of the distance from the primary vertex as measured using $\alpha$-decays of radioactive contaminations in the emulsion. The histogram is the expected efficiency calculated with the simulation.